Industrial Crops & Products 159 (2021) 113017

Contents lists available at ScienceDirect

Industrial Crops & Products

journal homepage: www.elsevier.com/locate/indcrop

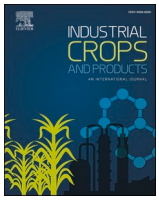

Acid hydrotropic fractionation of switchgrass at atmospheric pressure using maleic acid in comparison with *p*-TsOH: Advantages of lignin esterification

Chen Su [a,b], Kolby Hirth [b], Zhulan Liu [a], Yunfeng Cao [a], J.Y. Zhu [b,*]

[a] *Jiangsu Co-innovation Center for Efficient Processing and Utilization of Forest Resources, Jiangsu Provincial Key Lab Pulp & Paper Science and Technology, Nanjing Forestry University, Nanjing, 210037, China*
[b] *USDA Forest Service, Forest Products Laboratory, Madison, WI, USA*

ARTICLE INFO

Keywords:
Maleic acid fractionation
Lignin esterification
Lignin-containing cellulose nanofibrils (LCNFs)
Antioxidant activity
Structural characteristics

ABSTRACT

Switchgrass was fractionated using maleic acid (MA) as an acid hydrotrope in comparison with *p*-toluenesulfonic acid (*p*-TsOH) at atmospheric pressure. MA achieved more rapid and greater maximal dissolution of lignin and hemicelluloses (88 % and 63 %, respectively) than did *p*-TsOH (73 % and 55 %, respectively). MA esterified (carboxylated) the dissolved acid hydrotropic lignin (AHL) as evidenced by 2D ^{1}H-^{13}C HSQC NMR analysis, which improved AHL antioxidant ability compared with AHL from *p*-TsOH that is not carboxylated. MA also carboxylated the lignin and cellulose in the fractionated cellulosic water-insoluble solids (WIS), which significantly improved WIS enzymatic digestiblity for sugar production than did *p*-TsOH with the same level of delignification. It also improved the lignin lubrication effect to facilitate mechanical fibrillation of WIS into lignocellulosic nanofibrils. MA is an FDA-approved indirect food additive (21CFR175-177) with lower acidity and solubility than *p*-TsOH, which substantially benefits recycling and decreasing environmental impacts to achieve sustainability.

1. Introduction

Switchgrass (*Panicum virgatum* L.) is a perennial plant that can be grown on marginal land in many regions of the US and can be used for sustainable production of biomaterials, bioenergy, and platform biochemical (Schmer et al., 2008). Effective and sustainable fractionation of switchgrass into key building blocks, such as sugars, lignocellulosic nanomaterials, and easily processable lignin precursors, is key to this endeavor. Early fractionation techniques focusing on efficient production of sugar and biofuels through enzymatic saccharification achieved some level of success (Wyman et al., 2011; Zhang et al., 2013) but were not economical. Recent studies emphasized the valorization of lignin by improving process economics using various techniques such as ionic liquid (Liu et al., 2018), organic solvents (Luterbacher et al., 2015; Si et al., 2017), and molten salt (Li et al., 2018). These techniques have challenges, especially in chemical recovery or capital costs because of the corrosivity of the chemicals used at the designated operating temperatures. Practical implementation of new fractionation processes will require low chemical toxicity and corrosivity, chemical recyclability with decreased waste streams, and high selectivity to facilitate valorization of all major components of plant biomass, as well as cost-effective integration into existing capital structure.

Acid hydrotropic fractionation (AHF) of lignocelluloses was first demonstrated using an aromatic sulfonic acid, *p*-Toluenesulfonic acid (*p*-TsOH) (Chen et al., 2017; Ma et al., 2018b). AHF can rapidly solubilize lignin at atmospheric pressure and below boiling resulting in low degrees of condensation, which facilitates valorization through further depolymerization (Cai et al., 2020b; Wang et al., 2019a) or via direct utilization as polymers. Lignin separation can be achieved simply by diluting the fractionation liquor to below the minimal hydrotropic concentration (MHC) (Chen et al., 2017; Ma et al., 2018a). AHF has high selectivity in preserving cellulose. The dissolved hemicelluloses can be dehydrated into furans as a high-value chemical using the hydrotrope remaining in the fractionation liquor without additional catalyst (Cai et al., 2020a; Zhu et al., 2019). The hydrotrope can then be reused after distilling off the furans and reconcentration.

Recently, we discovered that maleic acid (MA) also has hydrotropic property toward wood lignin (Cai et al., 2020a). As a Food and Drug Administration (FDA)-approved indirect food additive (21CFR175-177, Code of Federal Regulations), MA has significant advantages over *p*-TsOH for reducing environmental impact. Furthermore, MA has a higher MHC than *p*-TsOH which can decrease water usage for lignin

* Corresponding author.
E-mail address: junyong.zhu@usda.gov (J.Y. Zhu).

https://doi.org/10.1016/j.indcrop.2020.113017
Received 11 June 2020; Received in revised form 9 October 2020; Accepted 12 October 2020
0926-6690/Published by Elsevier B.V.

precipitation. MA also has a lower water solubility at room temperature than *p*-TsOH which decreases water distillation for acid recovery (Cai et al., 2020b). As a weaker acid, MA is less corrosive than *p*-TsOH to significantly reduce capital and operating costs. In view of these advantages, it is desirable to compare MA with *p*-TsOH for fractionation of lignocelluloses. This study conducted a comparative evaluation of AHF fractionation of switchgrass using *p*-TsOH and MA. The study is focused on (1) using a reaction-kinetics-based severity factor to characterize AHF of switchgrass for process scale-up; and (2) comparing the performance of *p*-TsOH with that of MA for biorefining switchgrass in the production of cellulose nanomaterials, sugars, and lignin precursors. The results obtained from this work can be used for developing viable biomass biorefinery technology.

2. Materials and methods

2.1. Materials

Switchgrass was complimentarily provided by the Department of Biological Systems Engineering, University of Wisconsin-Madison. The switchgrass was Wiley-milled with a 1-cm mesh size screen. The materials that passed the screen were used for this study.

p-TsOH and MA of ACS reagent grade were purchased from Sigma-Aldrich (St. Louis, MO, USA). 2,2-diphenyl-1-picrylhydrazyl(DPPH) and 2,2′-azino-bis(3-ethylbenzothiazoline-6-sulfonic acid) (ABTS) diammonium salt of ACS high-performance liquid chromatography (HPLC) grade were also purchased from Sigma-Aldrich. A commercial complex cellulase, Cellic CTec3 (abbreviated CTec3), was complimentarily provided by Novozymes North America (Franklinton, NC, USA). The CTec3 had a cellulase activity of 217 FPU/mL.

2.2. Switchgrass fractionation and compositional analysis

Switchgrass fractionation experiments using aqueous *p*-TsOH and MA solutions were carried out at a biomass to acid solution ratio of 1:15 (w/w) under a range of conditions of concentration of 20–60 wt% at 60–120 ℃ for 20–120 min, as shown schematically in Fig. 1. These runs were denoted as P*xx*T*yy*t*zz* or M*xx*T*yy*t*zz* to represent the *p*-TsOH or MA concentration in *xx* wt% at *yy* ℃, and *zz* min. Aqueous *p*-TsOH or MA solutions were prepared in a conical flask by dissolving a desired amount of *p*-TsOH or MA in deionized (DI) water to make 200 g of acid solution. The flask was placed on a heat-controlled shaker (C-MAG HS7DS1, IKA, USA) to facilitate dissolution. 10 g in oven-dry (OD) weight of switchgrass were added into 150 g of the prepared *p*-TsOH or MA solution under constant stirring at the designed reaction temperature and time.

The chemical composition of *p*-TsOH and MA fractionated water-insoluble lignocellulosic solids (WIS) were determined by the Analytical Chemistry and Microscopy Laboratory at the USDA Forest Service, Forest Products Laboratory, Madison, WI, USA, using the two-step sulfuric acid hydrolysis method, as described previously (Luo et al., 2010). Briefly, lignocellulosic solids were hydrolyzed for 1 h in each of the two steps using sulfuric acid at 72 % (v/v) and 30 °C, and 3.6 % (v/v) at 120 °C, respectively. The balance between the unsolubilized solids and the ash determined from burning at 560 °C for 3 h was considered as lignin. The solubilized sugar streams were analyzed by an HPLC system (Ultimate 3000, ThermoFisher Scientific) equipped with a BioRad Aminex HPX-87H column (300 mm × 7.8 mm) operated at 60 °C and a refraction index detector (RI-101, Shodex) (Ma et al., 2018b; Zhou et al., 2013).

2.3. Preparation of switchgrass milled wood lignin (MWL)

Air-dried switchgrass was milled to pass 30 mesh in a Wiley mill (Model No. 2, Thomas Scientific, Swedesboro, NJ). The dried powder was then milled in a vibratory ball mill (PM100, Retsch, Haan, Germany) for 12 h (Holtman et al., 2006; Suzuki et al., 1998). The ball-milled powder was extracted by stirring in an aqueous dioxane solution of volumetric concentration 96 % with a solid-to-liquid ratio of 1:20 (g/mL) for 24 h. This procedure was repeated three times with fresh solvent. The mixture was filtered and washed with the same solvent until the filtrate was clear. Then, all filtrates were combined and evaporated under vacuum at 40 ℃ to remove dioxane. The solids were dried in a vacuum oven at 40 ℃ to obtain the crude MWL. The crude MWL was dissolved in 90 % acetic acid and precipitated by dropwise addition to water. The precipitate was washed, freeze-dried, and dissolved in dichloroethane/ethanol (2:1, v/v) mixture. The solution was precipitated by dropwise addition to ether, and the precipitate was filtered and washed with ether and petroleum ether and dried to obtain the purified switchgrass MWL.

2.4. Enzymatic hydrolysis

Enzymatic hydrolysis of fractionated WIS was performed in 125 mL conical flasks on a shaking bed incubator (Model 4450, Thermo Scientific, Waltham, MA, USA) at 200 rpm and 50 ℃ with WIS loading of 1%

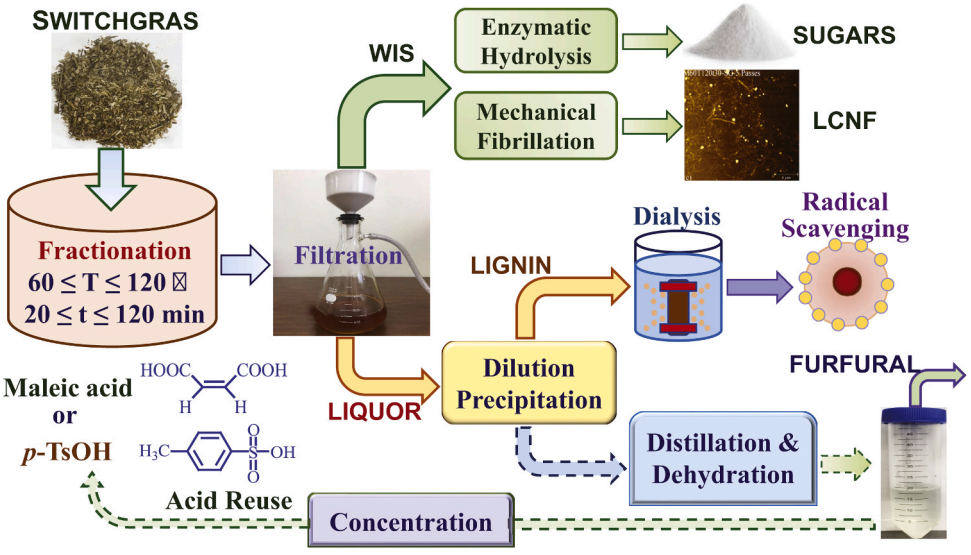

Fig. 1. Experimental schematic flow diagram showing hydrotropic fractionation, production of sugars and cellulose nanomaterials from fractionated cellulosic solids, furfural from dissolved xylan, and AHF lignin with low degree of condensation for valorization. Processes with dashed lines were not carried out in this work.

(w/v). 50 mM acetate buffer of pH 5.7, greater than the commonly used pH of 5.0, was used to buffer hydrolysis to decrease nonproductive cellulase binding to lignin as reported previously (Lan et al., 2013; Lou et al., 2013). CTec3 cellulase loading was 10 FPU/g cellulose. Aliquots of hydrolysate were taken at 2, 4, 6, 8, 10, 24, 48, 72, and 96 h during hydrolysis to obtain time-dependent sugar production. The samples were centrifuged at 10,000 rpm for 10 min and the supernatant was analyzed for glucose using a biochemistry analyzer (YSI 2900D, YSI Inc., Yellow Springs, Ohio, USA).

2.5. LCNF production and characterization

WISs from low severity fractionations were dispersed in DI water for 2 h and then disintegrated using a laboratory disintegrator (TMI, Ronkonkoma, NY, USA) at 0.5 wt% for 15,000 revolutions. The fiber suspensions were mechanically fibrillated into lignin-containing cellulosic nanofibrils (LCNFs) at approximately 0.5 wt% using a microfluidizer (M-11OEH, Microfluidics Corp., Westwood, MA, USA) and passed through two chambers in series with diameters of 200 and 87 μm, respectively, for five or nine passes at an operating pressure of 120 MPa.

The morphology of LCNFs was examined using an atomic force microscope (AFM) (CS-3230, AFM Workshop, Signal Hill, CA, USA). LCNFs were diluted to approximately 0.01 wt% and dispersed via sonication for 1 h, then stirred for 4 h at room temperature. A drop of the suspension was deposited on a clean mica plate and air-dried overnight at room temperature before AFM measurement. Height distribution was obtained by analyzing the AFM topographic images using Image-Pro Plus software (Media Cybernetics, Silver Spring, MD, USA).

LCNF Carboxyl group content was determined using conductometric titration, as described previously (Bian et al., 2017a). Briefly, an LCNF suspension containing 100 mg LCNFs was mixed with 100 mL of 1-mM NaCl solution and then titrated with continuous stirring using 10-mM NaOH, which was added dropwise every 30 s to allow time for equilibration before measuring conductivity. Conductance was measured using a conductivity meter (Model 35, YSI, Inc., Yellow Springs, Ohio, USA).

The surface charge of the LCNFs was measured using a zeta potential analyzer (Nanobrook Omni, Brookhaven Instruments, Holtville, NY, USA) at room temperature. The concentration of the suspension was approximately 0.05 g/L.

The water retention value (WRV) of LCNFs was measured following the standard test method SCAN-C 62:00 (SCAN, 2000), as described in our previous works (Gu et al., 2018; Luo and Zhu, 2011).

2.6. AHF lignin molecular weight determination using GPC

Acetylated lignin was prepared for gel permeation chromatography (GPC) analyses according to literature (Li et al., 2018; Yang et al., 2016). Briefly, 0.1 g freeze-dried lignin sample was dissolved in 2 mL of pyridine-acetic anhydride solution (1:1 vol). The solution was placed in a paper box to avoid light and incubated on a temperature-controlled shaker at 150 rpm and 40 ℃ for 72 h. The solution was added dropwise into 100 mL of ice water with continuous stirring to precipitate lignin acetate, which was filtered and washed with water and then freeze-dried. The various acetylated lignin preparations were dissolved in tetrahydrofuran (THF, HPLC grade) with a concentration of 1 mg/mL and analyzed by LC-20A GPC (Shimadzu, Japan) using an organic size-exclusion chromatography column (KF-804, 300 mm × 8 mm i.d., 7 μm), calibrated with polystyrene standards (peak average molecular weights (Mw) of 1000, 2000, 5000, 10,000, and 120,000 g/mol). The column was run at 40 ℃ and eluted with THF at a flow rate of 1 mL/min.

2.7. Nuclear magnetic resonance (NMR) spectroscopic analyses of lignin

^{31}P NMR and 2D ^{1}H-^{13}C heterogeneous single quantum correlation (HSQC) NMR of lignin samples were analyzed using a Bruker (Billerica, MA, USA) AVANCE 500 MHz spectrometer. For ^{31}P NMR analysis, 20 mg of nonacetylated lignin was dissolved in 0.5 mL anhydrous pyridine-d_5/$CDCl_3$ (1.6/1, v/v) solution. 100 μL of cyclohexanol (11.02 mg/mL, internal standard) and 100 μL chromium (III) acetylacetonate (5 mg/mL, relaxation regent), prepared using anhydrous pyridine-d_5/$CDCl_3$ solution, were mixed with lignin solution and then added to 60 μL phosphitylating regent (2-chloro-4,4,5,5-tetramethyl-1,2,3-dioxaphospholane), which was shaken at room temperature for 30 min, and then immediately analyzed. For 2D-HSQC NMR experiments, 70 mg of lignin were dissolved in 0.5 mL of dimethyl sulfoxide (DMSO)-d_6 as described previously (Chen et al., 2017). HSQC experiments were performed using the Bruker standard pulse program hsqcetgisisp2.2. Spectra were acquired using 40 scans and an interscan delay of 1 s for a total time of 3 h and used a 12-ppm sweep width in F2 (1 H) using 1024 data points for an acquisition time of 85 ms and a 215-ppm sweep width in F1 (^{13}C) using 512 increments with 50 % nonuniform sampling density. Data processing used Gaussian multiplication (LB -0.1, GB = 0.01) in F2 and squared consine bell (QSine SSB = 2) with zero-fill and linear forward prediction of 40 coefficients in F1 resulting in a 1024 × 1024 data matrix. Topspin 3.5pl7 was used for interactive integration of the cross peaks after the central DMSO solvent peak was referenced at δ ^{13}C, 39.5 ppm; δ ^{1}H, 2.49 ppm. Spectral images were colored using Adobe Illustrator CS6. Chemical structures were drawn using ChemDraw Pro 14.0.

2.8. Antioxidant activities of lignin

The antioxidant activities of lignin were evaluated by measuring the radical scavenging capacity of DPPH and ABTS (Jiang et al., 2018a). Briefly, the DPPH assay of concentration of 6×10^{-5} mol/L was prepared by dissolving in ethanol. The ABTS assay was prepared by reacting aqueous ABTS diammonium salt (7 mM) with aqueous 2.45 mM potassium persulfate and then allowing it to stand for 15 h in the dark at room temperature. Lignin samples were dissolved in dioxane/water (9:1, v/v) solution. The dissolved lignin was separately added into the DPPH and ABTS assays and reacted for 30 min and 6 min, respectively. The amount of DPPH and ABTS remaining in the assays was spectroscopically analyzed using a spectrophotometer (Model 8453, Agilent Technologies, Palo Alto, CA) at 517 nm and 734 nm, respectively.

3. Results and discussion

3.1. Component mass yield through AHF

The chemical composition and component yields of WISs from AHF under different conditions (Table S1) reveal that lignin and xylan dissolution increased with reaction severity for both *p*-TsOH and MA fractionations; however, the dissolution of glucan was low, below 20 %, for all runs. As reported previously (Ma et al., 2018b), acid hydrotropic fractionation can retain minerals on WIS, which is reflected by the reported high ash contents (Table S1).

Reaction severity-based kinetic analysis (Zhu et al., 2012) was effective in predicting xylan and lignin dissolution in AHF wood fractionation (Zhang et al., 2015; Zhu et al., 2019) to facilitate process scale-up (Zhou et al., 2015, 2013). The fraction of xylan, X_R, and lignin, L_R, retained on a WIS after AHF can be expressed by a combined hydrolysis factor (*CHF*) and a combined delignification factor (*CDF*), respectively, as follows:

$$X_R = (1 - \theta - \theta_R)e^{-CHF} + \theta \cdot e^{-f \cdot CHF} + \theta_R \quad (1a)$$

$$CHF = \exp(\alpha - \frac{E}{RT} + \beta C) \cdot C \cdot t \quad (1b)$$

$$L_R = (1 - \theta' - \theta'_R)e^{-CDF} + \theta' \cdot e^{-f' \cdot CDF} + \theta'_R \quad (2a)$$

$$\mathrm{CDF} = \exp\left(\alpha' - \frac{E'}{RT} + \beta' C\right) \cdot C \cdot t \quad (2b)$$

where C is the p-TsOH or MA molar concentrations (mol/L), $R = 8.314$ (J/mol/K) is the universal gas content, t is the reaction time in min, and T is reaction temperature in Kelvin. α, α', and β, β' are adjustable parameters; E and E' are apparent activation energy (J/mol), θ and θ' are the initial fraction of slow-reacting xylan and lignin, respectively. f and

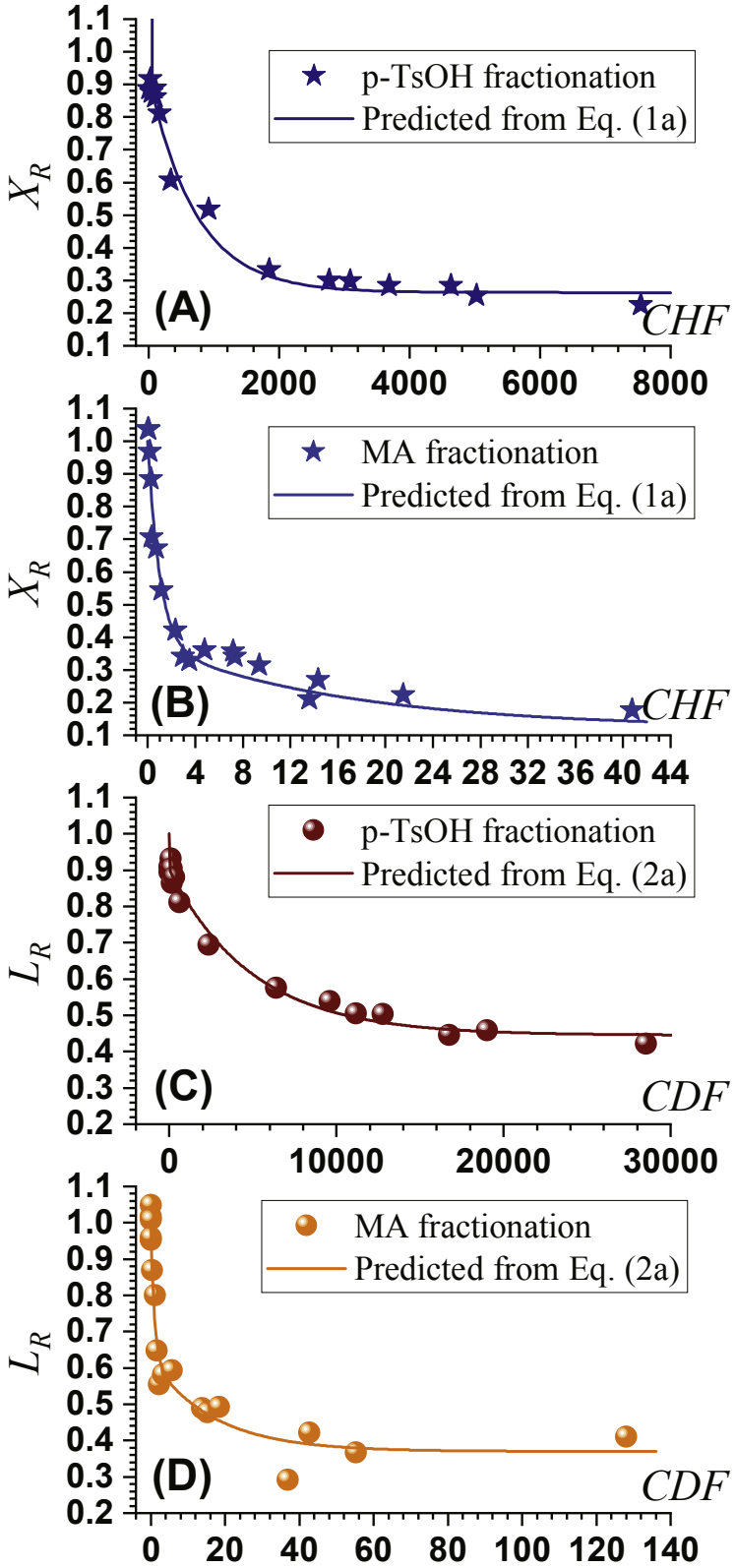

Fig. 2. Comparisons of xylan (A and B) and lignin (C and D) dissolution between two AHFs using p-TsOH and MA, along with their predictions based on reaction-severity-based kinetics.

f' are the ratios of reaction rates between slow and fast xylan and slow and fast lignin, respectively. θ_R and $\theta_{R'}$ are residual xylan and lignin, respectively. The fitting parameters (Table S2) indicated that the apparent activation energy E' for lignin dissolution is higher than E for xylan dissolution, which is consistent with the higher residual lignin $\theta_{R'}$ than residual xylan θ_R. Lignin dissolution also has a stronger dependence on acid concentrations, i.e., $\beta'_{MA} > \beta_{MA}$ and $\beta'_{p\text{-TsOH}} > \beta_{p\text{-TsOH}}$.

Excellent fittings of measured amounts of xylan and lignin retained in WISs to Eqs. (1a) and (2a) were obtained, as shown in Fig. 2. The results clearly demonstrate that AHF dissolutions of xylan and lignin, by both MA and *p*-TsOH, have a rapid phase followed by a slow, "long" phase to reach asymptotic values θ_R and $\theta_{R'}$ for xylan and lignin, respectively. Furthermore, both *p*-TsOH and MA dissolved most of the switchgrass xylan and lignin, or approximately two-thirds, during the first rapid phase, which is in agreement with an earlier study using poplar wood and *p*-TsOH (Zhu et al., 2019).

Comparing MA with *p*-TsOH, MA fractionation (MAHF) had a much sharper transition from the rapid phase to the slow phase than *p*-TsOH fractionation (PAHF). MA also dissolved more xylan and lignin than did *p*-TsOH (Fig. 2) and left lower amounts of residual xylan and lignin in WISs, i.e., $\theta_{R\text{-}MA} = 0.121 < \theta_{R\text{-}p\text{-}TsOH} = 0.370$ and $\theta_{R'\text{-}MA} = 0.263 < \theta_{R'\text{-}p\text{-}TsOH} = 0.445$ (Table S2), despite MA being a much weaker acid than *p*-TsOH. These observed differences in xylan and lignin dissolution suggest that these two hydrotropes are inherently different, which is subsequently explored further by analyzing the dissolved lignin and WIS.

The results in Fig. 2 also indicate that a desired degree of xylan or lignin dissolution can be obtained as long as the proper severity of *CDF* or *CHF* is used in the fractionation, independent of the individual reaction conditions. Therefore, using *CDF* and *CHF* aids process scale-up, especially if there are site-specific constraints on an individual condition(s). For example, low concentrations are usually desirable to decrease chemical recovery costs; therefore, a longer reaction time can be used to compensate for the low acid dosage.

3.2. AHF WISs for enzymatic sugar production

Several WISs from PAHF and MAHF were enzymatically hydrolyzed to compare the effectiveness of these two hydrotropes for sugar production from switchgrass. These samples were selected so that comparisons could be made among samples with similar lignin removal. Their lignin and xylan content and removal through AHF along with their substrate enzymatic digestibility (SED) are listed in Table 1. In general, increasing lignin removal increased SED for both MAHF and PAHF, as shown in Fig. 3A. The differences in SED of WISs from these two AHFs were negligible below lignin removal of approximately 40 %. However, at high lignin removal above 40 %, MAHF resulted in substantially greater SED than did PAHF. Comparing WIS M60T120t30 with WIS P60T80t90, with almost the same lignin and xylan removals of 57.8 % and 79.0 %, respectively, WIS M60T120t30 had a much greater SED of 78.5 % than did WIS P60T80t90 of 53.7 % (Fig. 3B). Even lower severity WISs M60T100t60 and M50T90t90, both of which had lower lignin and xylan removals than WIS P60T80t90, had greater SEDs (73.1 % and 57.3 %, respectively) than that from WIS P60T80t90 (53.7 %). This clearly indicates that factors other than WIS physical porosity (accessibility) created by dissolution of lignin and hemicelluloses affected SED.

Table 1
Lists of Lignin and xylan content of selected WISs, amounts of lignin and xylan removed through the AHF fractionation condition, and WIS substrate enzymatic digestibility (SED).

WIS [a]	Lignin content (%)	Lignin removal (%)	Xylan content (%)	Xylan removal (%)	SED @96 h (%)
P20T60t20	24.4	6.8	25.6	12.4	5.5
P40T80t60	22.7	42.4	14.5	56.8	51.0
P60T80t90	18.7	57.9	11.1	76.4	53.7
M30T70t90	24.7	13.1	21.7	12.7	9.6
M40T90t120	24.2	35.2	12.1	66.0	45.4
M50T90t90	22.2	41.8	11.9	67.2	57.3
M60T100t60	18.2	52.2	12.3	66.0	73.1
M60T120t30	17.2	57.8	8.1	79.0	78.5

[a] M*xx*T*yy*t*zz* or P*xx*T*yy*t*zz* stands for fractionation under MA or *p*-TsOH concentration at *xx* wt% and *yy* °C for *zz* min.

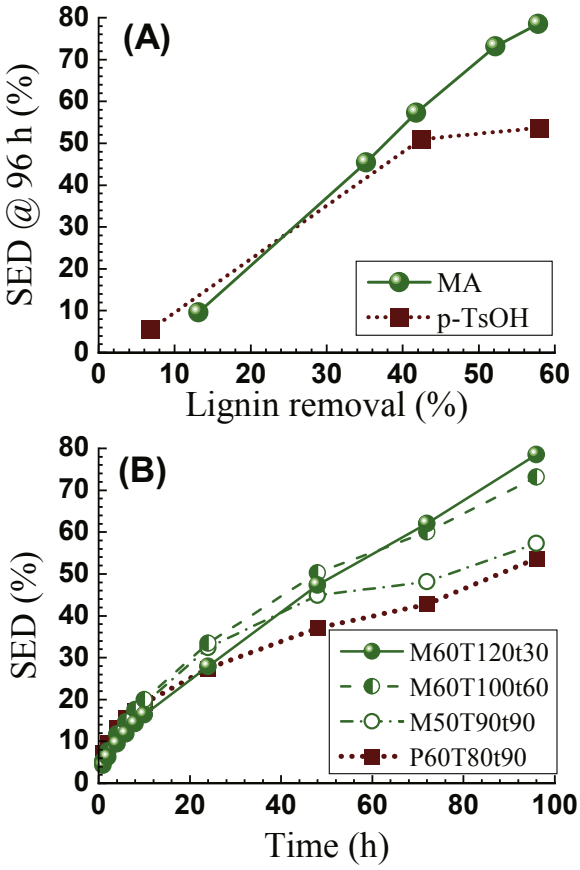

Fig. 3. Comparisons of enzymatic substrate digestibility (SED) between *p*-TsOH and MA fractionated WISs (CTec3 loading 10 FPU/g glucan with hydrolysis pH 5.7). (A): Effect of lignin removal; (B) Time-dependent SED profiles.

Lignin carboxylation at higher MAHF severities (Cai et al., 2020a), such as at lignin removal greater than 40 % (as will be discussed later in Table 2), contributed to the decrease in nonproductive cellulase binding to substrate lignin when enzymatic hydrolysis is conducted under elevated pH such pH = 5.7 in this study (Lan et al., 2013; Lou et al., 2013). This explains the significantly greater enzymatic digestibility of WISs from MAHF than WISs from PAHF that were not carboxylated, in agreement with our earlier studies using birch wood (Cai et al., 2020a). As shown in Fig. 3B, WIS P60T80t90 with higher lignin and xylan removal had a slightly greater initial hydrolysis rate than the WISs from MAHF within the first 10 h; however, the hydrolysis rate was decreased much more rapidly than that of the three WISs from MAHF, probably

Table 2
Water retention value (WRV), carboxyl group content, and surface charge of LCNFs.

LCNFs	WRV (%)	COOH (mmol/g)	ζ potential (mV)
P60T80t90−5	539	0.045 ± 0.007	−30.3 ± 2.2
M60T120t30−5	710	0.203 ± 0.010	−36.7 ± 1.4
P60T80t90−9	664	0.049 ± 0.008	−31.7 ± 2.0
M60T120t30−9	848	0.220 ± 0.011	−37.5 ± 3.6

because of the dominance of nonproductive cellulase binding in the later stage of hydrolysis. The hydrolysis rate of WIS M60T120t30 was almost unchanged at 96 h from the rate at 10 h, suggesting that nonproductive cellulase binding is negligible and SED can reach 95 % in another 24 h based on linear extrapolation of the data shown. This is a significant advantage of MAHF for enzymatic sugar production.

3.3. AHF WISs for producing LCNFs

Two AHF WISs P60T80t90 and M60T120t30 with very similar levels of lignin and xylan removal (Table 1) were compared for producing LCNFs. AFM images and AFM topography-measured fibril height probability density distributions are shown in Fig. 4. Lignin nanoparticles are clearly observable as both WISs had a relatively high lignin content of more than 17 % (Table 1). LCNFs produced using PAHF had greater height compared with LCNFs from MAHF under the same extent of fibrillation (numbers of passes through the microfluidizer). Increasing fibrillation decreased the average height and decreased the fibril networks as shown (comparing Fig. 4A with B and C with D). Mean LCNF height was decreased from 10.9 to 7.5 nm and from 8.8 to 6.0 nm by

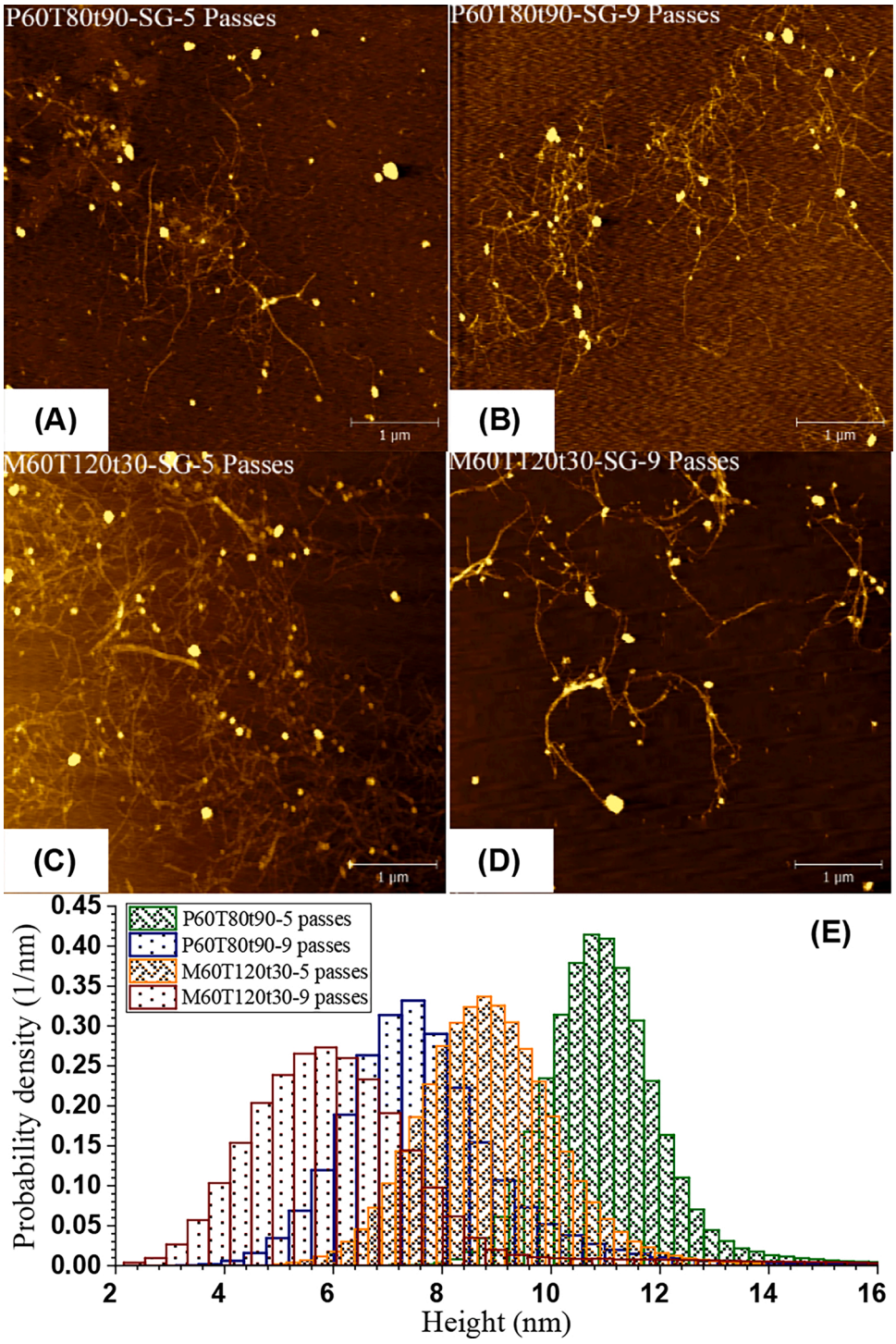

Fig. 4. AFM images of LCNFs from AHF WISs (A-D) using *p*-TsOH and MA and varied passes through microfluidization along with their AFM topography-measured LCNF height probability distributions. A: P60T80t90-5 P; B: P60T90t90-9 P; C: M60T120t30-5 P; D: M60T120t30-9 P; E: LCNF height distributions.

increasing the numbers of passes from 5 to 9 through the 87-μm chamber of the microfluidizer for *p*-TsOH- and MA-produced LCNFs (Fig. 4E), respectively.

The morphology of LCNF samples can also be indirectly evaluated using their WRV as we demonstrated in an earlier study (Gu et al., 2018) though surface chemistry also affects WRV. The WRV of a lignocellulosic material represents its interaction with water and total surface area (Luo et al., 2011) for samples with same surface chemistry. PAHF-produced LCNFs had a lower WRV than MAHF-produced LCNFs under the same extent of microfluidization as listed in Table 2. Increasing the extent of fibrillation increased WRV for both PAHF and MAHF LCNFs, in agreement with the AFM topographic measurements previously discussed.

Esterification (carboxylation) of lignin (Cai et al., 2020a) and cellulose (Fischer and Speier, 1895; Chen et al., 2016) by MA resulted in negatively charged WIS, which induced repulsion between fibrils and enhanced the role of lubrication that lignin plays in nanofibrillation (Ferrer et al., 2012; Spence et al., 2010) as observed previously (Bian et al., 2017b; Cai et al., 2020a). As listed in Table 2, LCNF samples from PAHF had a significantly lower amount of carboxyl groups (COOH) (less than 0.05 mmol/g) than LCNFs from MAHF because COOH content in natural lignocelluloses is very low and *p*-TsOH does not esterify lignin and cellulose. The two MA LCNF samples had COOH content of more than 0.2 mmol/g and a higher zeta-potential (ξ) of approximately −37 mV compared with −31 mV for the two LCNFs from *p*-TsOH (Table 2).

Although the titration method employed here cannot discern lignin esterification from cellulose esterification, our previous study indicated that COOH group content in CNFs derived from bleached kraft pulp fibers under a more severe hydrolysis condition (than the conditions employed in this study using MA) was only 0.06 mmol/g (Bian et al., 2017b); this is significantly lower than the values of over 0.2 mmol/g for the MA-LCNFs from the present study (Table 2) and strongly suggests that both lignin and cellulose in MA-LCNFs are esterified. This is also supported by the NMR measured higher COOH content of dissolved lignin (Table 4) than of LCNFs (Table 2).

3.4. Molecular weight distributions of dissolved lignin

GPC analysis of the lignin samples showed decreasing mean Mw as fractionation severity increased (Table 3). Previous works (Cai et al., 2020b; Cheng et al., 2019; Villaverde et al., 2009; Wang et al., 2019b) found that acidic fraction substantially depolymerized lignin, especially under severe fractionation conditions. The AHLs L-P20 and L-M30 from the mildest fractionation runs, using *p*-TsOH and MA with delignification of 6.8 % and 13.1 %, had fairly high Mw of 6674 and 8458 Da (Table 3), respectively, although these values were much lower than the 13,000 Da of switchgrass MWL. With increasing delignification to 42 %, the mean AHL Mw remained fairly high at 6060 and 7000 Da, respectively, for *p*-TsOH and MA fractionation (Table 3); however, the Mw distribution broadened as shown in Fig. 5. AHL L-M50, from a moderate severity M50T90t90 with delignification of 42 %, had a similar and slightly narrower distribution to that of switchgrass MWL and shifted toward the low Mw because of depolymerization. AHL L-P60 from *p*-TsOH fractionation with delignification of 58 % had a distinctive bimodal distribution, which reflects the competing reactions of depolymerization and repolymerization associated with the lower and higher Mw peaks at approximately 1180 and 2140 Da, respectively. The significant lignin condensation caused by repolymerization is also clearly reflected by the 2D NMR analyses as will be discussed later. By comparison, L-M60 from MAHF under M60T120t30 at the same level of delignification of 58 %, with a much lower degree of lignin condensation, has a single peak Mw distribution and fairly high Mw of 4840 Da.

3.5. AHF lignin chemical structure from ^{1}H-^{13}C HSQC NMR spectra

2D HSQC NMR was used to compare the structure of selected AHLs from *p*-TsOH and MA fractionation with switchgrass MWL, as shown in Fig. 6.

The assignments of main cross-signals of lignin (Table S3) and quantification of main chemical structures per 100 monomeric lignin units (100Ar) are based on literature (Capanema et al., 2004; Del Río et al., 2012; Li et al., 2018; Yelle et al., 2008). Correlation peaks from

Table 3
Amount of lignin substructure and lignin carbohydrate complex (LCC) linkages along with mean molecular weight (Mw) of MWL and AHL samples.

Fractionation	MWL	P20T60t20	P40T80t60	P60T80t90	M30T70t90	M50T90t90	M60T120t30
Lignin removal (%)		6.8	42.4	57.9	13.1	41.8	57.8
Lignin samples	MWL	L-P20	L-P40	L-P60	L-M30	L-M50	L-M60
Mw	13,091	6674	6066	3666	8458	7009	4841
Mn	4803	3106	2721	2299	3666	3708	3067
Mw/Mn	2.7	2.1	2.2	1.6	2.3	1.9	1.6
Interunit linkages[a]							
β−O−4' (A)	47.1	42.6	32.9	21.0	46.9	37.8	28.8
β−5' (B)	5.9	3.5	4.6	3.4	3.3	4.0	5.2
β−β' (C)	6.1	1.3	1.3	2.6	1.4	1.5	1.9
Condensed degree[c]	20.3	10.1	15.2	22.2	9.1	12.7	19.8
γ-esterification	6.8	5.2	3.3	2.7	15.3	33.5	46.8
HKα	ND	ND	2.5	11.7	ND	0.8	3.7
Aromatic units[b]							
S	32	41	44	49	30	36	38
S_{cond}	–	2	4	10	1	2	4
G	65	55	51	46	66	60	57
H	3	4	5	5	4	4	5
S/G ratio	0.49	0.75	0.86	1.07	0.45	0.60	0.67
***p*-Hydroxycinnamates**[b]							
p-coumarates	15.8	15.1	16.0	17.4	16.6	17.1	18.3
ferulates	4.0	2.3	2.1	2.2	1.3	1.8	1.7
Flavonoid[b]							
Tricin	4.2	1.1	0.4	0.4	0.6	0.4	0.4
LCC linkages							
PhGlc	3.9	2.2	1.0	1.1	1.5	1.5	1.5
BE	3.1	1.4	0.9	0.7	1.6	1.1	1.1

[a] Molar percentages (H + G + S = 100).
[b] Interunit linkages, *p*-coumarate, ferulate, and tricin molar contents as percentages of lignin content (H + G + S).
[c] Condensed degree, % = 100 * ($I_{Bα}$+ $I_{Cα}$) / (I_{A}+ $I_{Bα}$+ $I_{Cα}$).

Table 4
Quantification of the functional groups in lignin by ^{31}P NMR spectroscopy.

Samples	Aliphatic OH	Phenolic OH (mmol/g)				COOH (mmol/g)
		Syringyl Condensed OH	Guaiacyl OH	*p*-Hydroxyl OH	Total	
MWL	2.81	0.28	0.49	0.36	1.13	0.32
L-M30	2.56	0.29	0.31	0.31	0.91	0.33
L-M50	1.61	0.43	0.52	0.38	1.33	0.61
L-P40	1.60	0.48	0.58	0.39	1.45	0.29

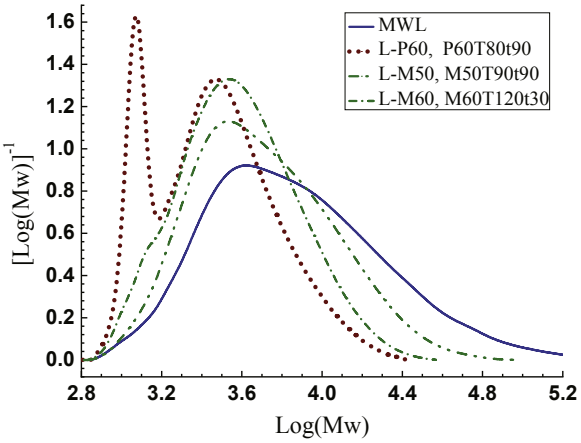

Fig. 5. Comparisons of molecular weight (Mw) distributions of the switchgrass AHLs and MWL.

methoxyl groups and β–O–4′ linkages (A) were most prominent in the side chain region of all lignin preparations, followed by phenylcoumarans (B) and resinols (C). Various signals associated with carbohydrates were also present, including β-D-xylopyranoside units (X), arabinofuranoside units (Ara), and 4-O-methyl-α-D-glucuronic acid units (U).

AHL from mild severity MAHF, L-M30 from M30T70t90, showed only small changes compared with MWL (Fig. 6A and B) with similar β–O–4′ linkages of approximately 47 % (Table 3), except the signal at δ_C/δ_H 63.5/(3.83, 4.30) ppm due to maleation at the γ-position Eγ(MA) overlapping with the signal at δ_C/δ_H 62.1/(4.23, 4.43) ppm (Fig. 6B) that is attributed to A'$_\gamma$–Est corresponding to the known acylated γ-position by *p*-coumarate of grass lignins (Balakshin et al., 2011; Wen et al., 2013a). The signals at δ_C/δ_H 128.0/6.2 and 132.9/6.4 ppm (Fig. 6B) are also attributed to lignin esterification at the γ-OH position by MA to form Eγ(MA), as confirmed by our earlier study (Cai et al., 2020a) and also identified in literature (Ralph et al., 2009; Zhou et al., 2019). AHL from PAHF at similar lignin removal resulted in decreased β–O–4′ linkages of 33 % (Table 3), which decreased with increasing *p*-TsOH fractionation severity (Table 3), in agreement with an earlier study using *p*-TsOH (Wang et al., 2020).

Increasing MAHF severity increased lignin esterification, as can be seen by comparing the signal intensity of Eγ(MA)$_{2,3}$ at δ_C/δ_H 128.0/6.2 and 132.9/6.4 ppm in the AHL 2D NMR spectra of L-M30 (Fig. 6B) with L-M50 (Fig. 6D), and decreased the signal of Aα because of increasing dissolution of hemicelluloses. The formation of Hibbert's ketones (HK) (δ_C/δ_H = 67.1/4.2 ppm, γ-position; δ_C/δ_H = 44.5/3.7 ppm, α-position) was visible from the spectrum of L-M50 (Fig. 6D) through the cleavage of β–O–4′ linkages because of acid-catalyzed formation of a benzylic cationic intermediate (Cheng et al., 2019; Li et al., 2018). The abundance of β–O–4′ linkages of L-M50 was decreased to approximately 38 % from 47 % for L-M30 (Table 3). S_{cond} signals can be clearly seen at δ_C/δ_H = 105.5/6.7 ppm in Figs. 6B-D.

Comparing AHF using MA with that using *p*-TsOH under moderate conditions, i.e., M50T90t90 with P40T80t60 with the same level of delignification of approximately 42 % (Table 1), L-P40 (Fig. 6C) from P40T80t60 is not esterified lacking the Eγ(MA) signals at δ_C/δ_H 128.0/6.2 and 132.9/6.4 ppm L-P40, and also has a slightly lower β–O–4′ linkage content of 33 % than the 38 % of L-M50 (Table 3). The higher degree of lignin condensation is also reflected from the more HK in L-P40 than in L-M50 as listed in Table 3. Similar trends of β–O–4′ linkage preservation, extent of lignin condensation, and HK formation were observed at elevated delignification of 58 % comparing MAHF under M60T120t30 and PAHF under P60T80t90 (Table 3, Fig. S1). At low AHF severities, MAHF under M30T70t90 removed more lignin than AHF under P20T60t20 using *p*-TsOH and also retained more β–O–4′ linkages (Table 3, Fig. S1). These comparisons indicate MAHF has better delignification selectivity in preserving more β–O–4′ linkages and preventing lignin condensation.

The lignin carbohydrate complex (LCC) linkages of phenyl glycoside (PhGlc) and benzyl ether (BE) were also identified in the zoomed-in 2D NMR spectra shown in Fig. 6. The PhGlc linkages in the MWL spectra showed three cross-signals at δ_C/δ_H 100.2−98.4/5.09−4.90 ppm (PhGlc1), 100.9−100.3/4.85−4.63 ppm (PhGlc2), and 102.0−101.5/4.92−4.79 ppm (PhGlc3) (Balakshin et al., 2011; Du et al., 2014). These peaks indicate that there are different kinds of carbohydrates associated with lignin by phenyl glycoside linkages. However, with increasing fractionation severity, some signals disappeared because of cleavage of some glycosidic bonds by AHF. The total amount of PhGlc in the switchgrass MWL was 3.9 per 100Ar. This decreased to 1.0 % as fractionation severity increased with the use of *p*-TsOH and increased to 1.5 % with the use of MA (Table 3). Benzyl ether, BE, shown in the region of δ_C/δ_H 85−80/5.4–4.0, has two types: (1) linkages between the α-position of lignin and primary OH groups of carbohydrates (BE1, δ_C/δ_H 82−80/4.7−4.5 ppm); and (2) linkages between the α-position of lignin and secondary OH groups of carbohydrates (BE2, δ_C/δ_H 82−80/5.1–4.9 ppm) (Jiang et al., 2018b). In a similar manner to PhGlc, the amount of BE decreased as fractionation severity increased. Again, the decrease in BE by MA is smaller than that by *p*-TsOH, i.e., from 3.1 for MWL to 0.7 and 1.1 for L-P60 and L-M60, respectively, with the same level of delignification (58 %) (Table 3), in agreement with an early study that showed smaller decreases of LCCs with decreased acidity (Wang et al., 2020).

3.6. ^{31}P NMR analysis

The main signals in ^{31}P NMR spectra (Fig. 7) were assigned and the content of OH in lignin was calculated as listed in Table 4 (in mmol/g lignin) according to previous literature (Granata and Argyropoulos, 1995). In general, both AHFs resulted in a decrease in aliphatic OH and an increase in phenolic OH and carboxyl groups. The decrease in aliphatic hydroxyl groups suggested that the aliphatic OH groups were oxidized and modified during MAHF, such as by the acid-catalyzed elimination reactions. The high content of the phenolic hydroxyl implies the cleavage of β-O-4′ linkages (Wen et al., 2013b). Under the same delignification of 42 %, AHL L-P40 from PAHF under P40T80t60 and L-M50 from MAHF from M50T90t90 had almost the same amount of aliphatic OH, while L-P40 had a slightly greater amount of phenolic OH than L-M50, suggesting that *p*-TsOH could break more β-O-4′ linkages and increase S and G phenolic hydroxyl groups than MA. Lignin esterification by MA increased the carboxyl group content in AHL from MAHF. L-M50 has almost twice the amount of carboxyl groups than

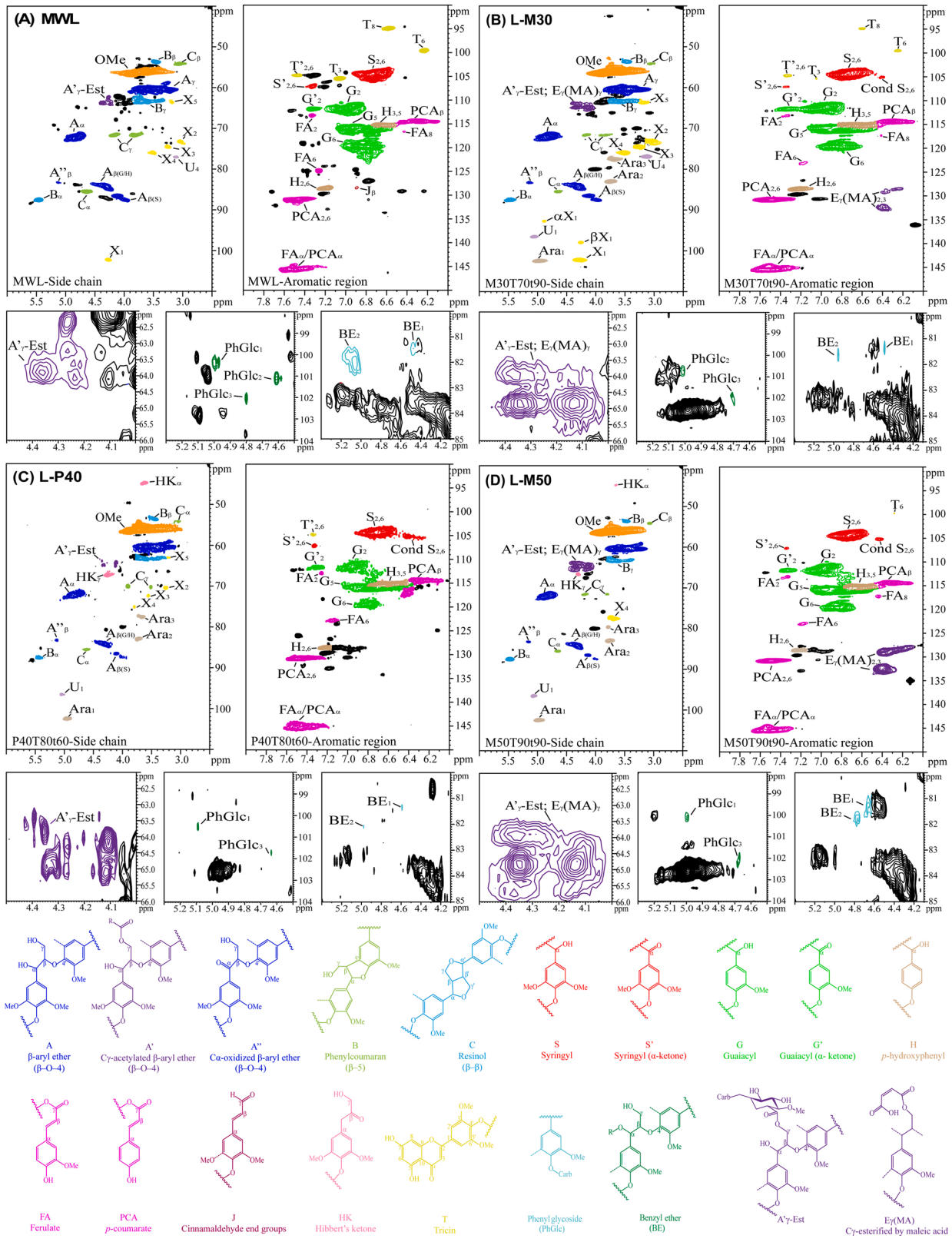

Fig. 6. ^{1}H-^{13}C 2D HSQC NMR spectra of MWL and AHLs from MA and *p*-TsOH hydrotropic fractionations. M*xx*T*yy*t*zz* or P*xx*T*yy*t*zz* stands for fractionation under MA or *p*-TsOH concentration at *xx* wt% and *yy* °C for *zz* min.

L-M30 had because of increased fractionation severity.

3.7. Assessment of radical scavenging ability

The antioxidant activities of AHLs from switchgrass were evaluated by examining their capacity to scavenge DPPH and ABTS radicals. All

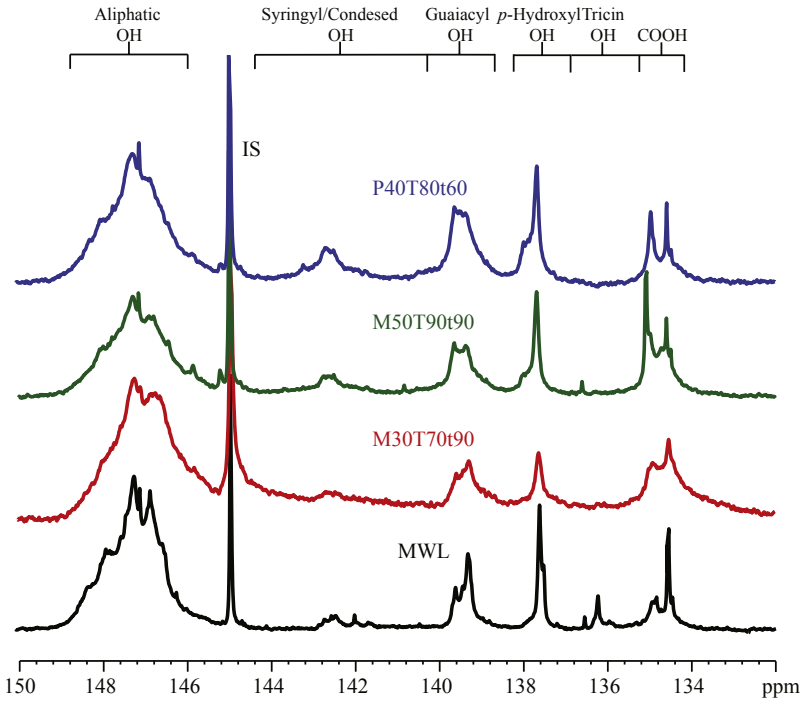

Fig. 7. Quantitative ^{31}P NMR spectra of the phosphitylated MWL and AHLs from different AHF conditions.

AHL samples were effective in scavenging DPPH and ABTS radicals as shown in Fig. 8. The scavenge capacity increases with AHL concentration (Niu et al., 2016). Both types of AHL had greater antioxidant activities than MWL toward both DPPH and ABTS radicals, especially toward the DPPH radical. In general, AHL from MAHF had greater scavenging capacity than AHL from PAHF toward both DPPH and ABTS radicals. However, the difference between these two types of AHL is not significant toward DPPH. At a relatively low dosage of 0.30 mg/mL, AHL L-M60 and L-M50 from MAHF can eliminate 90 % of both radicals in the prescribed time of 30 min and 6 min for DPPH and ABTS, respectively.

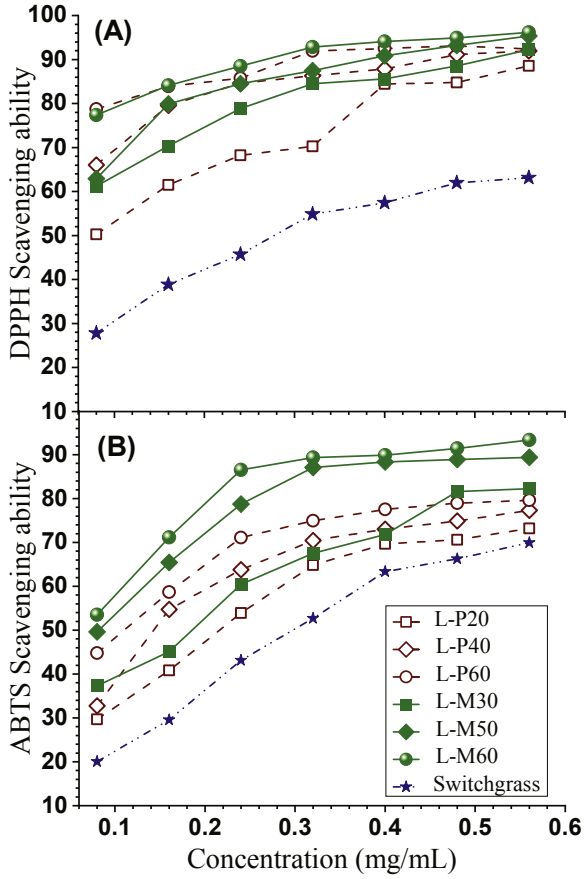

Fig. 8. Scavenging ability of AHLs toward DPPH (A) and ABTS radicals (B).

The differences in the lignin chemical structural are responsible for the observed difference in AHL antioxidant activity. The antioxidant activity of lignin mainly comes from the scavenging properties of its hydroxyl structure, including phenolic and carboxyl hydroxyl (Dizhbite et al., 2004; Jiang et al., 2018a, 2019). Lignin esterification by MAHF increased carboxyl group content, and the cleavage of ether aryl linkages increased phenolic OH content, as verified by ^{31}P NMR analysis (Table 4), which contributed favorably to improving antioxidant activity (Qin et al., 2018) as shown in Fig. 8.

4. Conclusions

This study demonstrated maleic acid hydrotropic fractionation (MAHF) of switchgrass at atmospheric pressure. MAHF resulted in carboxylated dissolved lignin with improved antioxidant activities and a lower degree of condensation. Lignin and cellulose carboxylation substantially improved enzymatic digestibility of the fractionated cellulosic water-insoluble solids (WIS) and facilitated mechanical fibrillation of WIS into lignocellulosic nanofibrills in comparison with WIS from *p*-TsOH fractionation under the same level of delignification, but without esterification. MA is an FDA-approved indirect food additive (21CFR175-177) with lower acidity and solubility than *p*-TsOH and has substantial advantages in recycling and decreasing environmental impacts to achieve sustainability.

CRediT authorship contribution statement

Su conducted most of the experiments including fractionation, enzymatic hydrolysis, mechanical fibrillation, lignin sample preparation, and also contributed to draft of the manuscript. Zhu initiated the research work, design the experiments, conducted data analyses and

rewrote most of the manuscript. Hirth conducted 2D ^{1}H-^{13}C HSQC NMR analyses and data analyses. Liu and Cao conducted ^{31}P NMR and assist n lignin antioxidant experiment.

Declaration of Competing Interest

The authors declare that they have no known competing financial interests or personal relationships that could have appeared to influence the work reported in this paper.

The Corresponding author Zhu is a co-inventor of Maleic acid hydrotropic fractionation.

Acknowledgements

We thank Professor Kevin Shinners of the Department of Biological Systems Engineering at the University of Wisconsin-Madison for complimentarily providing us the switchgrass. We are grateful for the financial support from the National Natural Science Foundation of China (No. 31670591). A Project Funded by the National First-class Disciplines (PNFD), Priority Academic Program Development (PAPD) of Jiangsu Higher Education Institution and Doctorate Fellowship Foundation of Nanjing Forestry University and Postgraduate Research & Practice Innovation Program of Jiangsu Province (KYCX17-0834). This work was conducted while Chen Su was a visiting PhD student at the USDA Forest Service, Forest Products Laboratory (FPL). We also acknowledge Fred Matt for conducting carbohydrate analyses, Kolby Hirth for conducting NMR analyses, and Rolland Gleisner for preparing switchgrass, all of whom are from FPL.

Appendix A. Supplementary data

Supplementary material related to this article can be found, in the online version, at doi:https://doi.org/10.1016/j.indcrop.2020.113017.

References

Balakshin, M., Capanema, E., Gracz, H., Chang, H., Jameel, H., 2011. Quantification of lignin-carbohydrate linkages with high-resolution NMR spectroscopy. Planta 233 (6), 1097–1110.

Bian, H., Chen, L., Dai, H., Zhu, J.Y., 2017a. Effect of fiber drying on properties of lignin containing cellulose nanocrystals and nanofibrils produced through maleic acid hydrolysis. Cellulose 24 (10), 4205–4216.

Bian, H., Chen, L., Dai, H., Zhu, J.Y., 2017b. Integrated production of lignin containing cellulose nanocrystals (LCNC) and nanofibrils (LCNF) using an easily recyclable dicarboxylic acid. Carbohydr. Polym. 167, 167–176.

Cai, C., Hirth, K., Gleisner, R., Lou, H., Qiu, X., Zhu, J.Y., 2020a. Maleic acid as a dicarboxylic acid hydrotrope for sustainable fractionation of wood at atmospheric pressure and ≤ 100 °C: mode and utility of lignin esterification. Green Chem. 22 (5), 1605–1617. https://doi.org/10.1039/C9GC04267A.

Cai, C., Li, J., Hirth, K., Huber, G.W., Lou, H., Zhu, J.Y., 2020b. Comparison of two acid hydrotropes for sustainabl fractionation of birch wood. ChemSusChem 13, 4649–4659. https://doi.org/10.1002/cssc.202001120.

Capanema, E.A., Balakshin, M.Y., Kadla, J.F., 2004. A comprehensive approach for quantitative lignin characterization by NMR spectroscopy. J. Agric. Food Chem. 52 (7), 1850–1860.

Chen, L., Dou, J., Ma, Q., Li, N., Wu, R., Bian, H., Yelle, D.J., Vuorinen, T., Fu, S., Pan, X., Zhu, J.Y., 2017. Rapid and near-complete dissolution of wood lignin at ≤ 80 °C by a recyclable acid hydrotrope. Sci. Adv. 3 (9), e1701735.

Chen, L., Zhu, J.Y., Baez, C., Kitin, P., Elder, T., 2016. Highly thermal-stable and functional cellulose nanocrystals and nanofibrils produced using fully recyclable organic acids. Green. Chem. 18, 3835–3843. https://doi.org/10.1039/c6gc00687f.

Cheng, J., Hirth, K., Ma, Q., Zhu, J., Wang, Z., Zhu, J.Y., 2019. Toward sustainable and complete wood valorization by fractionating lignin with low condensation using an acid hydrotrope at low temperatures (≤ 80 °C). Ind. Eng. Chem. Res. 58, 7063–7073. https://doi.org/10.1021/acs.iecr.9b00931.

Del Río, J.C., Rencoret, J., Prinsen, P., Martínez, A.T., Ralph, J., Gutiérrez, A., 2012. Structural characterization of wheat straw lignin as revealed by analytical pyrolysis, 2D-NMR, and reductive cleavage methods. J. Agric. Food Chem. 60 (23), 5922–5935.

Dizhbite, T., Telysheva, G., Jurkjane, V., Viesturs, U., 2004. Characterization of the radical scavenging activity of lignins—natural antioxidants. Bioresour. Technol. 95 (3), 309–317.

Du, X., Perez-Boada, M., Fernandez, C., Rencoret, J., del Rio, J.C., Jimenez-Barbero, J., Li, J., Gutierrez, A., Martinez, A.T., 2014. Analysis of lignin-carbohydrate and lignin-lignin linkages after hydrolase treatment of xylan-lignin, glucomannan-lignin and glucan-lignin complexes from spruce wood. Planta 239 (5), 1079–1090.

Ferrer, A., Quintana, E., Filpponen, I., Solala, I., Vidal, T., Rodríguez, A., Laine, J., Rojas, O.J., 2012. Effect of residual lignin and heteropolysaccharides in nanofibrillar cellulose and nanopaper from wood fibers. Cellulose 19 (6), 2179–2193.

Fischer, E., Speier, A., 1895. Darstellung der ester. Berichte Der Dtsch. Chem. Gesellschaft 28 (3), 3252–3258.

Granata, A., Argyropoulos, D.S., 1995. 2-chloro-4,4,5,5-tetramethyl-1,3,2-dioxaphospholane, a reagent for the accurate determination of the uncondensed and condensed phenolic moieties in Lignins. J. Agric. Food Chem. 43 (6), 1538–1544.

Gu, F., Wang, W., Cai, Z., Xue, F., Jin, Y., Zhu, J.Y., 2018. Water retention value for characterizing fibrillation degree of cellulosic fibers at micro and nanometer scales. Cellulose 25 (5), 2861–2871.

Holtman, K.M., Chang, H.M., Jameel, H., Kadla, J.F., 2006. Quantitative 13C NMR characterization of milled wood lignins isolated by different milling techniques. J. Wood Chem. Technol. 26 (1), 21–34.

Jiang, B., Zhang, Y., Gu, L., Wu, W., Zhao, H., Jin, Y., 2018a. Structural elucidation and antioxidant activity of lignin isolated from rice straw and alkalioxygen black liquor. Int. J. Biol. Macromol. 116, 513–519.

Jiang, B., Zhang, Y., Guo, T., Zhao, H., Jin, Y., 2018b. Structural characterization of lignin and lignin-carbohydrate complex (LCC) from Ginkgo shells (Ginkgo biloba L.) by comprehensive NMR spectroscopy. Polymers 10 (7).

Jiang, B., Zhang, Y., Zhao, H., Guo, T., Wu, W., Jin, Y., 2019. Structure-antioxidant activity relationship of active oxygen catalytic lignin and lignin-carbohydrate complex. Int. J. Biol. Macromol. 139, 21–29.

Lan, T.Q., Lou, H., Zhu, J.Y., 2013. Enzymatic saccharification of lignocelluloses should be conducted at elevated pH 5.2–6.2. Bioenergy Res. 6 (2), 476–485.

Li, N., Li, Y., Yoo, C.G., Yang, X., Lin, X., Ralph, J., Pan, X., 2018. An uncondensed lignin depolymerized in the solid state and isolated from lignocellulosic biomass: a mechanistic study. Green Chem. 20 (18), 4224–4235.

Liu, E., Li, M., Das, L., Pu, Y., Frazier, T., Zhao, B., Crocker, M., Ragauskas, A.J., Shi, J., 2018. Understanding lignin fractionation and characterization from engineered switchgrass treated by an aqueous ionic liquid. ACS Sustain. Chem. Eng. 6 (5), 6612–6623.

Lou, H., Zhu, J.Y., Lan, T.Q., Lai, H., Qiu, X., 2013. pH-Induced lignin surface modification to reduce nonspecific cellulase binding and enhance enzymatic saccharification of lignocelluloses. ChemSusChem 6 (5), 919–927.

Luo, X., Gleisner, R., Tian, S., Negron, J., Horn, E., Pan, X.J., Zhu, J.Y., 2010. Evaluation of mountain beetle infested lodgepole pine for cellulosic ethanol production by SPORL pretreatment. Ind. Eng. Chem. Res. 49 (17), 8258–8266.

Luo, X., Zhu, J., Gleisner, R., Zhan, H., 2011. Effects of wet-pressing-induced fiber hornification on enzymatic saccharification of lignocelluloses. Cellulose 18 (4), 1055–1062.

Luo, X., Zhu, J., 2011. Effects of drying-induced fiber hornification on enzymatic saccharification of lignocelluloses. Enzyme Microb. Technol. 48 (1), 92–99.

Luterbacher, J.S., Azarpira, A., Motagamwala, A.H., Lu, F., Ralph, J., Dumesic, J.A., 2015. Lignin monomer production integrated into the γ-valerolactone sugar platform. Energy Environ. Sci. 8 (9), 2657–2663.

Ma, Q., Chen, L., Wang, W., Yang, R., Zhu, J.Y., 2018a. Direct production of lignin nanoparticles (LNPs) from wood using p-toluenesulfonic acid in an aqueous system at 80°C: characterization of LNP morphology, size, and surface charge. Holzforschung 72 (11), 933–942.

Ma, Q., Zhu, J., Gleisner, R., Yang, R., Zhu, J.Y., 2018b. Valorization of wheat straw using a recyclable hydrotrope at low temperatures (≤90 °C). ACS Sustain. Chem. Eng. 6, 14480–14489. https://doi.org/10.1021/acssuschemeng.8b03135.

Niu, H., Song, D., Mu, H., Zhang, W., Sun, F., Duan, J., 2016. Investigation of three lignin complexes with antioxidant and immunological capacities from Inonotus obliquus. Int. J. Biol. Macromol. 86, 587–593.

Qin, Z., Zhang, Z.-G., Liu, H.-M., Qin, G.-Y., Wang, X.-D., 2018. Acetic acid lignins from Chinese quince fruit (Chaenomeles sinensis): effect of pretreatment on their structural features and antioxidant activities. RSC Adv. 8 (44), 24923–24931.

Ralph, S.A., Ralph, J., Landucci, L., 2009. NMR database of lignin and cell aall model compounds. USDA Forest Products Laboratory, Madison, WI. FPL/DFRC NMR Database -April 2009 (Ed.) U.F.P. Lab. Madison, WI. http://www.glbrc.org/databases_and_software/nmrdatabase/NMR_DataBase_2009_Complete.pdf.

Schmer, M.R., Vogel, K.P., Mitchell, R.B., Perrin, R.K., 2008. Net energy of cellulosic ethanol from switchgrass. PNAS 105, 464–469.

Si, X., Lu, F., Chen, J., Lu, R., Huang, Q., Jiang, H., Taarning, E., Xu, J., 2017. A strategy for generating high-quality cellulose and lignin simultaneously from woody biomass. Green Chem. 19 (20), 4849–4857.

Spence, K.L., Venditti, R.A., Rojas, O.J., Habibi, Y., Pawlak, J.J., 2010. The effect of chemical composition on microfibrillar cellulose films from wood pulps: water interactions and physical properties for packaging applications. Cellulose 17 (4), 835–848.

Suzuki, S., Shintani, H., Park, S.Y., Saito, K., Laemsak, N., Okuma, M., Iiyama, K., 1998. Preparation of binderless boards from steam exploded pulps of oil palm (Elaeis guineensis Jaxq.) fronds and structural characteristics of lignin and wall polysaccharides in steam exploded pulps to be discussed for self-bindings. Holzforschung 52 (4), 417–426.

Villaverde, J.J., Li, J., Ek, M., Ligero, P., de Vega, A., 2009. Native lignin structure of Miscanthus x giganteus and its changes during acetic and formic acid fractionation. J. Agric. Food Chem. 57 (14), 6262–6270.

Wang, Z., Qiu, S., Hirth, K., Cheng, J., Wen, J., Li, N., Fang, Y., Pan, X., Zhu, J.Y., 2019a. Preserving both lignin and cellulose chemical structures: flow-through acid hydrotropic fractionation (AHF) at atmospheric pressure for complete wood

valorization. ACS Sustain. Chem. Eng. 7, 10808–10820. https://doi.org/10.1021/acssuschemeng.9b01634.
Wang, Z., Qiu, S., Hirth, K., Cheng, J., Wen, J., Li, N., Fang, Y., Pan, X., Zhu, J.Y., 2019b. Preserving both lignin and cellulose chemical structures: flow-through acid hydrotropic fractionation at atmospheric pressure for complete wood valorization. ACS Sustain. Chem. Eng. 7 (12), 10808–10820.
Wang, W., Gu, F., Zhu, J.Y., Sun, K., Cai, Z., Yao, S., Wu, W., Jin, Y., 2020. Fractionation of herbaceous biomass using a recyclable hydrotropic p–toluenesulfonic acid (p–TsOH)/choline chloride (ChCl) solvent system at low temperatures. Ind. Crops Prod. 150, 112423. DOI: 10.1016/j.indcrop.2020.112423.
Wen, J.L., Sun, S.L., Xue, B.L., Sun, R.C., 2013a. Recent advances in characterization of lignin polymer by solution-state nuclear magnetic resonance (NMR) methodology. Materials 6 (1), 359–391.
Wen, J.L., Sun, S.N., Yuan, T.Q., Xu, F., Sun, R.C., 2013b. Fractionation of bamboo culms by autohydrolysis, organosolv delignification and extended delignification: understanding the fundamental chemistry of the lignin during the integrated process. Bioresour. Technol. 150, 278–286.
Wyman, C.E., Balan, V., Dale, B.E., Elander, R.T., Falls, M., Hames, B., Holtzapple, M.T., Ladisch, M.R., Lee, Y.Y., Mosier, N., Pallapolu, V.R., Shi, J., Thomas, S.R., Warner, R. E., 2011. Comparative data on effects of leading pretreatments and enzyme loadings and formulations on sugar yields from different switchgrass sources. Bioresour. Technol. 102 (24), 11052–11062.
Yang, X., Li, N., Lin, X., Pan, X., Zhou, Y., 2016. Selective cleavage of the aryl ether bonds in lignin for depolymerization by acidic lithium bromide molten salt hydrate under mild conditions. J. Agric. Food Chem. 64 (44), 8379–8387.
Yelle, D.J., Ralph, J., Frihart, C.R., 2008. Characterization of nonderivatized plant cell walls using high-resolution solution-state NMR spectroscopy. Magn. Reson. Chem. 46 (6), 508–517.
Zhang, D.S., Yang, Q., Zhu, J.Y., Pan, X.J., 2013. Sulfite (SPORL) pretreatment of switchgrass for enzymatic saccharification. Bioresour. Technol. 129, 127–134.
Zhang, J., Gu, F., Zhu, J.Y., Zalesny, R.S., 2015. Using a combined hydrolysis factor to optimize high titer ethanol production from sulfite-pretreated poplar without detoxification. Bioresour. Technol. 186, 223–231.
Zhou, H., Zhu, J.Y., Luo, X., Leu, S.-Y., Wu, X., Gleisner, R., Dien, B.S., Hector, R.E., Yang, D., Qiu, X., Horn, E., Negron, J., 2013. Bioconversion of beetle-killed lodgepole pine using SPORL: process scale-up design, lignin coproduct, and high solids fermentation without detoxification. Ind. Eng. Chem. Res. 52 (45), 16057–16065.
Zhou, H., Zhu, J.Y., Gleisner, R., Qiu, X., Horn, E., 2015. High titer ethanol and lignosulfonate productions from SPORL pretreated poplar at pilot-scale. Front. Energy Res. 3, 16.
Zhou, H., Xu, J.Y., Fu, Y., Zhang, H., Yuan, Z., Qin, M., Wang, Z., 2019. Rapid flow-through fractionation of biomass to preserve labile aryl ether bonds in native lignin. Green Chem. 21 (17), 4625–4632.
Zhu, W., Houtman, C.J., Zhu, J., Gleisner, R., Chen, K., 2012. Quantitative predictions of bioconversion of aspen by dilute acid and SPORL pretreatments using a unified combined hydrolysis factor (CHF). Process. Biochem. 47 (5), 785–791.
Zhu, J., Chen, L., Gleisner, R., Zhu, J.Y., 2019. Co-production of bioethanol and furfural from poplar wood via low temperature (≤90 °C) acid hydrotropic fractionation (AHF). Fuel 254, 115572. https://doi.org/10.1016/j.fuel.2019.05.155.